## Avoided quantum criticality in exact numerical simulations of a single disordered Weyl cone

Justin H. Wilson , David A. Huse , 2,3 S. Das Sarma, and J. H. Pixley 1

1 Department of Physics and Astronomy, Center for Materials Theory, Rutgers University, Piscataway, New Jersey 0854, USA

2 Physics Department, Princeton University, Princeton, New Jersey 08544, USA

3 Institute for Advanced Study, Princeton, New Jersey 08540, USA

4 Condensed Matter Theory Center and Joint Quantum Institute, Department of Physics, University of Maryland,

College Park, Maryland 20742, USA



(Received 2 June 2020; accepted 26 August 2020; published 8 September 2020)

Existing theoretical works differ on whether three-dimensional Dirac and Weyl semimetals are stable to a short-range-correlated random potential. Numerical evidence suggests the semimetal to be unstable, while some field-theoretic instanton calculations have found it to be stable. The differences go beyond method: the continuum field-theoretic works use a single, perfectly linear Weyl cone, while numerical works use tight-binding lattice models which inherently have band curvature and multiple Weyl cones. In this work, we bridge this gap by performing exact numerics on the same model used in analytic treatments, and we find that all phenomena associated with rare regions near the Weyl node energy found in lattice models persist in the continuum theory: The density of states is nonzero and exhibits an avoided transition. In addition to characterizing this transition, we find rare states and show that they have the expected behavior. The simulations utilize sparse matrix techniques with formally dense matrices; doing so allows us to reach Hilbert space sizes upwards of  $10^7$  states, substantially larger than anything achieved before.

DOI: 10.1103/PhysRevB.102.100201

The stability of phase transitions in the presence of non-perturbative effects of rare regions is a central question in modern statistical mechanics [1–3]. These problems fall into two classes; the first is the case of "clean" critical point perturbed by disorder, and the second consists of transitions driven solely by disorder. The latter case is less understood as both the existence of the transition and the rare region effects arise from the same origin: randomness. As a result, rare regions could destabilize one of the two phases turning a putative transition into a crossover.

The problem of three-dimensional short-range disordered Dirac and Weyl semimetals [4] is a quintessential example of a disorder-driven transition that has a nontrivial interplay with nonperturbative, rare-region effects [3,5-35]. Initial work using large N [5] and a perturbative renormalization group [6] found that Dirac and Weyl semimetals are stable to the presence of weak disorder and possess a quantum phase transition into a diffusive metal phase; this is indicated by the order parameter, the density of states at zero energy, becoming nonanalytic at the transition. On the other hand, rare-region arguments and mean-field instanton calculations [10] argued that nonperturbative effects lead to a finite density of states at the Weyl (or Dirac) node for infinitesimal disorder strength, thus destabilizing the semimetallic phase.

Confirming the rare-region expectation, extensive numerical simulations on lattice models of Dirac and Weyl semimetals have found nonperturbative rare eigenstates that round the perturbative transition into a crossover dubbed an avoided quantum critical point (AQCP) [24,25,27,30,31] with an analytic density of states. A phenomenological, field-theoretic description of the AQCP has been put forth [28], and

additional support for the rare-region scenario comes from T-matrix calculations of the quasiparticle lifetime [27], conductivity [29], and the prediction of a nonzero density of states from a continuous distribution of scattering approach [32]. Last, by replacing the randomness by quasiperiodicity, rare regions are removed entirely from the problem, and a genuine quantum phase transition between a Weyl semimetal and a diffusive metal is seen [36], albeit with no randomness in the model.

Recently, continuum field-theoretic work that considered fluctuations about the instanton saddle point for a single Weyl cone have challenged the rare-region scenario [33]. In Ref. [33] the authors find that while rare regions exist, they do not destabilize the semimetallic phase because the density of states at the Weyl node remains zero for nonzero disorder. An immediate conclusion of this scenario is that the perturbative quantum critical point remains stable to disorder; in the present work, we directly investigate this question in a numerical realization of a single Weyl cone. Previous simulations [24,25,27,30,31] have at least two Weyl cones (due to the fermion doubling theorem [37]), internode scattering, and band curvature effects; their conclusions, strictly speaking, do not apply to a single Weyl cone with a linear dispersion at all energies. While some numerical results exist on the conductance in the limit of a single Weyl cone [8,15], no rare region effects have been reported. Additionally, the existing numerical techniques that have been highly successful in reaching large enough system sizes to observe rare region effects rely on sparse matrices (that naturally occur in local lattice models) and efficient matrix-vector multiplication not directly applicable to treat

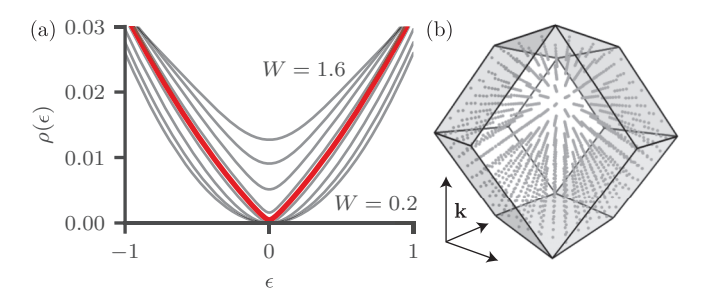


FIG. 1. (a) Density of states  $\rho(\epsilon)$  as a function of energy  $\epsilon$  for various different values of disorder W ranging from W=0.2 to W=1.6 in steps of 0.2. The red curve is for W=0.9 and is close to the avoided transition. Far enough away from zero energy this behaves as  $\rho(\epsilon) \sim |\epsilon|$ , consistent with avoided criticality. (b) Depiction of the fcc momentum space lattice and the rhombic dodecahedron Brillouin zone.

disordered continuum models. Therefore, the important issue remains open on whether the conflicting conclusions about the existence of QCP versus AQCP have perhaps been obtained in different models. To resolve this, we employ exact numerics which necessarily include disorder realizations past those considered in Ref. [33] as they can contain numerous rare regions [24].

In the present Rapid Communication, we numerically study a disordered, single Weyl node by adapting sparse matrix-vector routines to work in the continuum. Technically, we achieve this by using fast Fourier transforms to act with the disorder potential in its diagonal real-space basis (similar to Ref. [38]). Importantly, the relevant sparse matrix algorithms which scale with (single-particle) Hilbert space dimension  ${\cal N}$ only increases from  $\mathcal{N}$  to  $\mathcal{N}(\log \mathcal{N})^3$  in three dimensions. To treat the continuum limit, we consider two controlled ways to discretize momentum space. First, we demonstrate the existence of rare regions in a model of a disordered, single Weyl cone. Second, we study the density of states near the Weyl node. We demonstrate avoidance of the perturbative transition; the density of states near this avoided transition is finite and remains an analytic function of energy and disorder near the Weyl node.

In Fig. 1(a), we show an example of the density of states  $\rho(\epsilon)$  as a function of energy  $\epsilon$  and disorder strengths W across the AQCP  $W_c$ . Approaching the AQCP, the  $\rho(\epsilon)$  scaling goes from  $\sim \epsilon^2$  to  $\sim |\epsilon|$  scaling at the (avoided) transition, consistent with the renormalization group expectation (z=3/2). However, this scaling does not persist to zero energy due to the nonzero density of states at  $\epsilon=0$ . As we track the zero-energy density of states  $\rho(0)$  for  $W < W_c$ , we find that  $\rho(0)$  is nonzero (converged with system size) and decreases in an exponential fashion, thus ruling out the stability of the semimetal phase. Importantly, all of our conclusions are unaffected by the discretization of the continuum. We conclude that AQCP survives the continuum single-cone limit.

Continuum model and numerical implementation. The model for a single disordered Weyl cone takes the form

$$\mathcal{H} = -i\hbar v_F \boldsymbol{\sigma} \cdot \boldsymbol{\nabla} + V(\mathbf{r}), \ \langle V(\mathbf{r} + \mathbf{R})V(\mathbf{r}) \rangle = W^2 e^{-R^2/\xi^2}, \tag{1}$$

where  $\langle \cdots \rangle$  represents the disorder average, and  $V(\mathbf{r})$  is a Gaussian random variable with zero mean. Without loss of

generality, we take  $v_F = 1 = \hbar$  and  $\xi = 1$ . For simulation purposes, we use the momentum space version of the problem where

$$\mathcal{H}_{\mathbf{k},\mathbf{k}'} = \boldsymbol{\sigma} \cdot \mathbf{k} (2\pi)^3 \delta(\mathbf{k} - \mathbf{k}') + V(\mathbf{k} - \mathbf{k}'), \tag{2}$$

the Gaussian disorder in the potential takes the form [39]

$$\langle V(\mathbf{k})V(\mathbf{k}')^* \rangle = W^2 \pi^{3/2} e^{-(1/4)k^2} (2\pi)^3 \delta(\mathbf{k} - \mathbf{k}'),$$
 (3)

and we define the Fourier transform such that  $\Psi(\mathbf{k}) = \int d^3x \, \Psi(\mathbf{x}) e^{-i\mathbf{k}\cdot\mathbf{x}}$ .

To discretize the problem, we construct a grid in momentum space characterized by three lattice vectors  $\mathbf{b}_i$  defined as columns of a matrix B. Momentum is found by a vector of integers **n** via  $\mathbf{k_n} = \delta k B(\mathbf{n} + \boldsymbol{\varphi})$  where  $\delta k = \frac{2\pi}{Na}$  for length scale a, number of grid points with linear dimension N, and offset  $\varphi \in [0, 1)^3$ . The length scale a is related to a real-space lattice spacing, Na to a system size, and we have periodic boundary conditions in real space. We consider two different momentum-space lattices: cubic and face-centered cubic (fcc). The fcc lattice provides the densest packing of spheres in three dimensions, allowing us to approximate the continuum more accurately for a given number of momentum-space grid points. For a cubic (momentum-space) lattice B is the identity, a is the lattice constant, and L = aN is the system size, but for a fcc lattice,  $B_{ij} = 1/2$  if  $i \neq j$  and  $B_{ii} = 0$ , the real-space lattice is body-centered cubic (bcc) occupying a rhombohedron with side length  $L = \sqrt{3aN}$  and angle between sides  $\alpha = \arccos(-1/3)$ . Similarly, the constructed grid determines the momentum space cutoff  $\Lambda$  by half the size of the linear dimension. For cubic discretization,  $\Lambda = \frac{\pi}{a}$  with a cubic cutoff around  $\boldsymbol{k}=\boldsymbol{0}$  while for the fcc discretization  $\Lambda = \frac{\pi}{\sqrt{2a}}$  with a rhombic dodecahedron cutoff around  $\mathbf{k} = 0$ , as depicted in Fig 1(b).

To discretize the Hamiltonian, we consider its action on a wave function

$$\mathcal{H}\Psi = \int \frac{d^3k'}{(2\pi)^3} \mathcal{H}_{\mathbf{k},\mathbf{k'}} \Psi(\mathbf{k'}) \approx \sum_{\mathbf{n'}} H_{\mathbf{n}\mathbf{n'}} \psi_{\mathbf{n'}}, \qquad (4)$$

where  $H_{\mathbf{n}\mathbf{n}'} \equiv \frac{\det(B)}{(Na)^3} \mathcal{H}_{\mathbf{k_n},\mathbf{k'_n}}$  and  $\psi_{\mathbf{n}} \equiv \Psi(\mathbf{k_n})$ . Discretization affects the Dirac delta function such that  $\delta(\mathbf{k_n} - \mathbf{k_{n'}}) \approx \frac{(Na)^3}{(2\pi)^3 \det(B)} \delta_{\mathbf{n}\mathbf{n'}}$ . This simplifies the kinetic term and discretizes the correlator in Eq. (3),

$$\langle V_{\mathbf{n}}V_{\mathbf{n}'}^* \rangle = W^2 \pi^{3/2} e^{-(1/4)(\delta k B \mathbf{n})^2} \frac{(Na)^3}{\det(B)} \delta_{\mathbf{n}\mathbf{n}'},$$
 (5)

where  $V_{\mathbf{n}} \equiv V(\delta k B \mathbf{n})$ . This correlator is achieved by [40]

$$V_{\mathbf{n}} = W z_{\mathbf{n}} \sqrt{\frac{(Na)^3}{\det(B)}} \pi^{3/2} e^{-(1/4)(\delta k B \mathbf{n})^2},$$
 (6)

where  $z_{\mathbf{n}}$  are Gaussian independent and identically distributed random complex numbers with  $\langle z_{\mathbf{n}} \rangle = 0$  and  $\langle z_{\mathbf{n}'}^* z_{\mathbf{n}} \rangle = \delta_{\mathbf{n}\mathbf{n}'}$ . To ensure V is Hermitian, we find the inversion operator for our lattice P and identify  $z_{\mathbf{n}} = z_{P\mathbf{n}}^*$  and make sure inversion symmetric points are real valued. We also impose  $V_0 = 0$  to avoid random spatially uniform shifts in the potential.

The discretized Hamiltonian is

$$H_{\mathbf{n}\mathbf{n}'} = \delta k \, \boldsymbol{\sigma} \cdot B(\mathbf{n} + \boldsymbol{\varphi}) \delta_{\mathbf{n}\mathbf{n}'} + \frac{\det(B)}{(Na)^3} V_{\mathbf{n} - \mathbf{n}'}. \tag{7}$$

This matrix as written is *dense*, but to take advantage of numerical techniques that only require matrix-vector multiplication, we consider how this acts on a vector  $\psi_n$ . First, the kinetic part is block diagonal, but the potential acts as a convolution. To implement a convolution, we need the three-dimensional Fourier transform of  $V_n$ . The result is a linear operator

$$\frac{\det(B)}{(aN)^3} \sum_{\mathbf{n'}} V_{\mathbf{n}-\mathbf{n'}} \psi_{\mathbf{n'}} = \frac{\det(B)}{a^3} \mathcal{F}[\mathcal{F}^{-1}[V_{\mathbf{n}}] \mathcal{F}^{-1}[\psi_{\mathbf{n}}]], \quad (8)$$

where  $\mathcal{F}$  is a three-dimensional fast Fourier transform (FFT). The FFT is, in a sense, returning us to real space where the potential is diagonal, but for our purposes, we consider it a tool for the application of the convolution. As Lanczos and the kernel polynomial method (KPM) [41] based approaches for sparse matrices scale like  $\sim \mathcal{N}$  (for matrix size  $\mathcal{N}$ ) the inclusion of the FFT only increases the computational cost to  $\mathcal{N}(\log \mathcal{N})^3$ , which keeps the algorithm sufficiently fast. Thus, our approach provides an efficient way to utilize matrix-vector routines to study inhomogeneous continuum models.

Using an FFT introduces a notion of Brillioun zones (BZs). For any finite BZ there is a discontinuity in the kinetic energy at the edge of the BZ due to the fermion doubling theorem: There ought to be a second Weyl fermion at the BZ edge with infinite velocity (but our finite grid never picks it up). Further, the convolution acts across the BZ, connecting  $\mathbf{k}$  points that are far from each other in the continuum but close in a periodic BZ. We expect that this only affects the high-energy behavior and does not affect the low-energy regime of interest that we are probing near E = 0. To confirm this, we compare two models with different cutoff physics—(1) the cubic lattice and (2) the fcc lattice—and we find that there is qualitatively no difference in the low-energy physics we study [39]. We illustrate the fcc lattice in Fig. 1(b).

Finally, if we stochastically sample  $\varphi$ , we reproduce the continuous density of states for the continuum system; all finite size effects are then from the discretization of  $V(\mathbf{k})$ . Physically, a nonzero  $\varphi$  is usually associated with twisted boundary conditions in real space.

Defining H as a linear operator allows us to take advantage of numerical techniques that only involve matrix-vector multiplication such as Lanczos and the KPM [41]. Lanczos is used to obtain eigenvectors near zero energy  $\epsilon=0$ , and we obtain averaged density of states

$$\rho_{\rm dis}(\epsilon) = \left\langle \frac{1}{2N^3} \sum_{n} \delta(\epsilon - \epsilon_n) \right\rangle,\tag{9}$$

with the KPM. To relate the density of states of the discretized Hamiltonian to its continuum counterpart, a measure factor is required from  $d^3k \approx (\delta k)^3 \det(B)$  which leads to  $\rho(\epsilon) = \frac{\det(B)}{a^3} \lim_{L,\Lambda \to \infty} \rho_{\mathrm{dis}}(\epsilon)$  for fixed W.

The KPM method uses a Chebyshev expansion to order  $N_C$ , leading to a density of states  $\rho_{N_C}(\epsilon)$  [39] which behaves as a convolution of the exact  $\rho_{\rm dis}(\epsilon)$  with a Gaussian of width  $\delta\epsilon = \frac{\pi\Delta}{N_C}$  and bandwidth  $\Delta$  of H. We probe the scaling of  $\rho_{N_C}(0)$  with  $N_C$  to assess the low-energy behavior of  $\rho(\epsilon)$ . Precisely, assuming the density of states is analytic, we Taylor expand

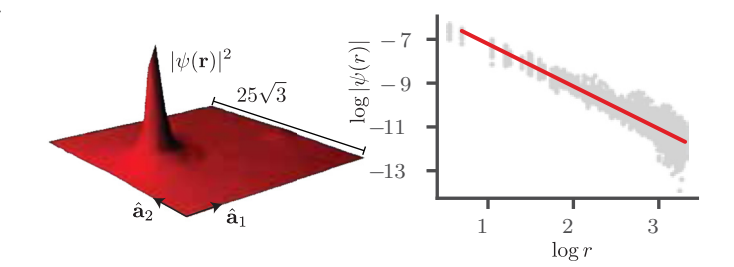


FIG. 2. Properties of a rare wave function computed with the fcc model with  $L=25\sqrt{3}$ ,  $\Lambda=\frac{\pi}{\sqrt{2}}$ , and a disorder strength below the AQCP  $W=0.7 < W_c(\Lambda) \approx 0.9$ . The energy of the state is  $\epsilon=0.0168$  but can made to pass smoothly through zero energy with a small perturbation of the disorder potential [39]. Left: The probability density of a rare wave function for a cut through the real-space bcc lattice where  $\hat{\bf a}_1$  [ $\hat{\bf a}_2$ ] is in the (1,-1,1) [(-1,1,1)] direction and  ${\bf r}=n_1{\bf a}_1+n_2{\bf a}_2+22{\bf a}_3$ . Right: A scatter plot of the wave function as a function of the distance to its maximum value demonstrating a clear power-law decay with  $|\psi({\bf r})| \sim 1/r^{1.94}$  for this rare state.

 $\rho(\epsilon)$  to find

$$\rho_{N_C}(0) = \rho(0) + \frac{1}{2}\rho''(0) \left(\frac{\pi \Delta}{N_C}\right)^2 + \cdots, \qquad (10)$$

and at the perturbative critical point, if we have  $\rho(\epsilon) \sim |\epsilon|$ , then

$$\rho_{N_C}(0) \sim \frac{1}{N_C} \quad \text{and} \quad \rho_{N_C}''(0) \sim N_C.$$
(11)

We also numerically compute  $\rho_{N_C}''(0)$  directly from the KPM expansion [25].

Finding rare states. We begin by finding a low-energy rare state in the weak disorder regime, i.e., below the avoided transition. We use Lanczos on  $H^2$  to find states that are not in the perturbative "Dirac peaks" [24]; such an example is shown in Fig. 2 that is power-law bound to the region (at  $\mathbf{r}_0$ ) of uncharacteristically high disorder strength. The rare wave function decays like  $\psi(\mathbf{r}) \sim 1/|\mathbf{r} - \mathbf{r}_0|^{\alpha}$ , where  $\alpha = 1.94$  in excellent agreement with the analytic prediction at the saddle point  $\alpha = 2$ . In summary, the rare wave function we have found here shares all of the same characteristics as in lattice model simulations, and we find that they are not any more difficult to find.

Behavior of the density of states. We now turn to a detailed analysis of the density of states. To get accurate results we average over a large number of disorder samples ranging from 2500 to 25 000 and analyze the zero-energy density of states following Eq. (10) to extract  $N_C$ -independent estimates of  $\rho(0)$  and  $\rho''(0)$  [39]. We use  $\rho''(0)$  to determine whether the density of states becomes nonanalytic, which would imply  $\rho''(0) \to \infty$ . In addition to the  $N_C$ -independent estimate of  $\rho''(0)$  we also compute it directly at fixed  $N_C$  within the KPM [25] which we denote as  $\rho''_{N_C}(0)$ . Note that, if the critical point exists it implies the scaling  $\rho_{N_C}(0) \sim 1/N_C$  and  $\rho''_{N_C}(0) \sim N_C$ . We test for this scaling by plotting  $N_C \rho_{N_C}(0)$  vs W; if it holds, then different  $N_C$  curves should intersect at one common point. However, as shown in Fig. 3(a), we find that no such crossing occurs; instead, each increasing pair of

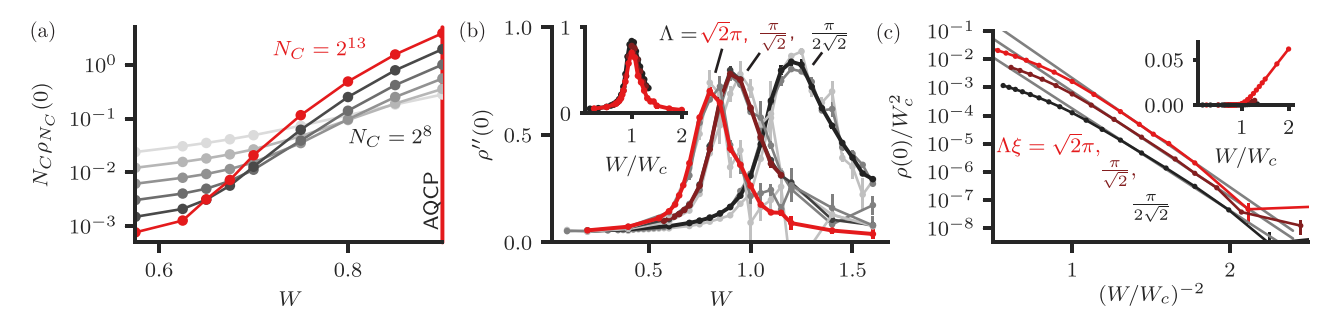


FIG. 3. Demonstrating the avoided transition and finite density of states. (a) From lightest to darkest each curve represents  $N_C=2^8$  to  $2^{13}$  in multiples of two  $(\Lambda=\pi/\sqrt{2} \text{ and } L=160\sqrt{3})$ . Other measures of the avoided criticality put  $W_c=0.9$  but we see that there is no saturation of  $N_C\rho_{N_C}(0)$  as we would expect from scaling with  $N_C$  at the quantum critical point. (b) We fit  $\rho_{N_C}(0)$  to Eq. (10) to extract  $\rho(0)$  and  $\rho''(0)$  in the  $N_C\to\infty$  limit [39]. We find for each cutoff studied, a peak in  $\rho''(0)$  saturated in system size (all gray curves are smaller system sizes  $L\Lambda\sqrt{2}/\pi=32\sqrt{3}$ ,  $64\sqrt{3}$ ,  $128\sqrt{3}$  and for  $\Lambda=\pi/\sqrt{2}$  we include  $L=160\sqrt{3}$ ). (b) Inset: Normalized with respect to the peak value ( $W_c=0.8,0.9,1.2$  left to right), the peaks line up well with each other, displaying a weak cut-off dependence. (c) We find  $\rho(0)$  is well fit by the rare-region form in Eq. (12) over approximately four orders of magnitude (gray lines). The data as plotted are converged in system size, as the gray curves indicate in (b) and as expanded upon in the Supplemental Material for (c) [39]. The inset shows the same data on a linear scale.

 $N_C$ 's intersects at smaller values of W, indicating the absence of a transition at the lowest energy scales.

Our second piece of evidence for the avoided transition is the strongly rounded peak in  $\rho''(0)$ , as shown in Fig. 3(b). We find that  $\rho''(0)$  is converged in system size (gray curves indicate smaller system sizes), not singular, and weakly dependent on the cutoff. Thus, we find that the density of states remains an analytic function of W and  $\epsilon$  at the Weyl node, except for an expected essential singularity at W=0 due to the nonperturbative disorder effects. The location of the maximum of the peak provides an accurate estimate of the avoided transition  $W_c(\Lambda)$  [24,25] that also agrees with the estimate based on the apparent scaling  $\rho(\epsilon) \sim |\epsilon|$ .

Tracking the zero-energy density of states for decreasing W below the avoided transition, we converge the  $N_C$ -independent  $\rho(0)$  in system size [39] to an exponentially small but nonzero value. As shown in Fig. 3(c), we find that the converged value of  $\rho(0)$  is well described by the results of the saddle-point instanton expectation [10],

$$\rho(0) = a(\Lambda) \exp[-b(W_c(\Lambda)/W)^2]. \tag{12}$$

Impressively, the data fit to this form extends over three to four orders of magnitude in  $\rho(0)$  depending on the cutoff. We find that all of the results share a common slope (with the fitted value ranging from  $b=8.3\pm0.7$  to  $b=8.9\pm1.1$  where the error is mostly due to  $W_c$  error) and the offset [i.e., the prefactor  $a(\Lambda)$ ] is cut-off dependent. Thus, as  $\rho(0)$  is converged in system size [Fig. 3(c)] and  $N_C$ , it is finite in the thermodynamic limit and increases with increasing cutoff. These results imply that rare regions have induced a nonzero density of states for any finite value of W and below the avoided transition, Eq. (12) describes it.

Finally, we present  $\rho_{N_C}''(0)$  directly computed from the KPM expansion to demonstrate any rounding from performing fits to Eq. (10) is weak and the lack of divergence of  $\rho''(0)$  is *intrinsic* to the problem. As shown in Fig. 4(a) we find that the peak in  $\rho_{N_C}''(0)$  grows with  $N_C$  but at the largest  $N_C$ 's the increase is minor, demonstrating saturation with  $N_C$ . For clarity and to test the critical scenario  $\rho_{N_C}''(0) \sim N_C$ , we plot the

peak value of  $\rho_{N_C}''(0)$  as a function of  $N_C$  in Fig. 4(b). We find that the peak is saturating with  $N_C$  (independent of the kind of discretization of the continuum) and does not come close to the critical scaling expectation. It is useful to contrast the rise in  $\rho_{N_C}''(0)$  with the quasiperiodic limit of the model [36], which has an actual transition and the divergence in  $\rho_{N_C}''(0)$  manifests as an increase over six orders of magnitude. In contrast, in the present model, the peak barely rises over one order of magnitude. The transition is strongly avoided.

Discussion. The physical role of rare states in causing a nonzero density of states appears unchanged from lattice models [24,25,27,30,31], and stands in contrast to analytic results [33]. The analytic work suggests that a single spherical potential (e.g., one rare state) cannot lead to a density of states at zero energy. However, the exact numerics have configurations with multiple rare states, which produce long-range tunneling matrix elements that are inversely proportional to the square of the distance between them [10,24]. On the other hand, to make a direct comparison of a single rare event (Fig. 2) and those of Ref. [33] the vector of angles  $\varphi$  (used in simulations) ought to be physically considered; it can be

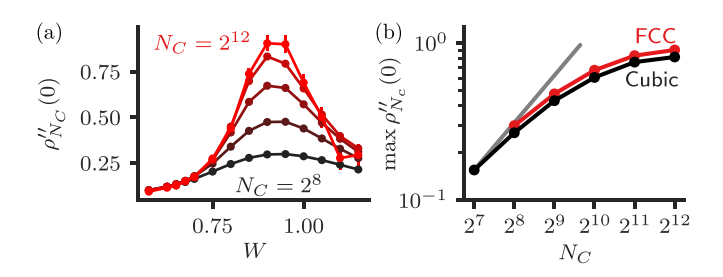


FIG. 4. Convergence of the peak of  $\rho_{N_C}''(0)$  at the AQCP. (a)  $N_C$  dependence of the second derivative of the density of states for the fcc model. (b) A plot of the peak saturated  $\rho_{N_C}''(0)$  data for both fcc and cubic data. Data at fixed  $N_C$  are converged in system size [39]. We see that they do not match the scaling we would expect from a true quantum critical point  $\rho_{N_C}''(0) \propto N_C$  (gray line). The fcc data has  $\Lambda = \pi/\sqrt{2}$  and  $L = 160\sqrt{3}$  while the cubic data has  $\Lambda = \pi$  and L = 160.

mapped *exactly* to a Bloch wave vector where the disorder potential on an  $N \times N \times N$  lattice is repeated infinitely in space. In this paradigm, even single rare states map to an infinite band of rare states, and the saturation of density of states with system size indicates that this band does not become sparser for larger supercells (i.e., larger N). Therefore, the density of rare states participating in these bands remains constant.

Acknowledgments. We thank A. Altland and M. Bucchold for illuminating conversations. D.A.H. was supported in part by a Simons Fellowship and by DOE Grant

No. DE-SC0016244. S.D.S. is supported by the Laboratory for Physical Sciences and Microsoft. J.H.P. is supported by NSF CAREER Grant No. DMR-1941569. The authors acknowledge the following research computing resources that have contributed to the results reported here: The University of Maryland supercomputing resources [42], the Beowulf cluster at the Department of Physics and Astronomy of Rutgers University; and the Office of Advanced Research Computing (OARC) at Rutgers, The State University of New Jersey [43], for providing access to the Amarel cluster.

- [1] T. Vojta, Rare region effects at classical, quantum and nonequilibrium phase transitions, J. Phys. A **39**, R143 (2006).
- [2] K. Agarwal, E. Altman, E. Demler, S. Gopalakrishnan, D. A. Huse, and M. Knap, Rare-region effects and dynamics near the many-body localization transition, Ann. Phys. (Leipzig) 529, 1600326 (2017).
- [3] S. V. Syzranov and L. Radzihovsky, High-dimensional disorder-driven phenomena in Weyl semimetals, semiconductors, and related systems, Annu. Rev. Condens. Matter Phys. 9, 35 (2018).
- [4] N. P. Armitage, E. J. Mele, and A. Vishwanath, Weyl and Dirac semimetals in three-dimensional solids, Rev. Mod. Phys. 90, 015001 (2018).
- [5] E. Fradkin, Critical behavior of disordered degenerate semiconductors. II. Spectrum and transport properties in mean-field theory, Phys. Rev. B 33, 3263 (1986).
- [6] P. Goswami and S. Chakravarty, Quantum Criticality between Topological and Band Insulators in 3+1 Dimensions, Phys. Rev. Lett. 107, 196803 (2011).
- [7] K. Kobayashi, T. Ohtsuki, K.-I. Imura, and I. F. Herbut, Density of States Scaling at the Semimetal to Metal Transition in Three Dimensional Topological Insulators, Phys. Rev. Lett. 112, 016402 (2014).
- [8] B. Sbierski, G. Pohl, E. J. Bergholtz, and P. W. Brouwer, Quantum Transport of Disordered Weyl Semimetals at the Nodal Point, Phys. Rev. Lett. **113**, 026602 (2014).
- [9] B. Roy and S. Das Sarma, Diffusive quantum criticality in three-dimensional disordered Dirac semimetals, Phys. Rev. B 90, 241112(R) (2014); Erratum: Diffusive quantum criticality in three-dimensional disordered Dirac semimetals [Phys. Rev. B 90, 241112(R) (2014)], 93, 119911 (2016).
- [10] R. Nandkishore, D. A. Huse, and S. L. Sondhi, Rare region effects dominate weakly disordered three-dimensional Dirac points, Phys. Rev. B 89, 245110 (2014).
- [11] J. H. Pixley, P. Goswami, and S. Das Sarma, Anderson Localization and the Quantum Phase Diagram of Three Dimensional Disordered Dirac Semimetals, Phys. Rev. Lett. 115, 076601 (2015).
- [12] A. Altland and D. Bagrets, Effective Field Theory of the Disordered Weyl Semimetal, Phys. Rev. Lett. **114**, 257201 (2015).
- [13] S. V. Syzranov, L. Radzihovsky, and V. Gurarie, Critical Transport in Weakly Disordered Semiconductors and Semimetals, Phys. Rev. Lett. 114, 166601 (2015).
- [14] S. V. Syzranov, V. Gurarie, and L. Radzihovsky, Unconventional localization transition in high dimensions, Phys. Rev. B 91, 035133 (2015).

- [15] B. Sbierski, E. J. Bergholtz, and P. W. Brouwer, Quantum critical exponents for a disordered three-dimensional Weyl node, Phys. Rev. B 92, 115145 (2015).
- [16] J. H. Pixley, P. Goswami, and S. Das Sarma, Disorder-driven itinerant quantum criticality of three-dimensional massless Dirac fermions, Phys. Rev. B 93, 085103 (2016).
- [17] M. Gärttner, S. V. Syzranov, A. M. Rey, V. Gurarie, and L. Radzihovsky, Disorder-driven transition in a chain with power-law hopping, Phys. Rev. B **92**, 041406(R) (2015).
- [18] S. Liu, T. Ohtsuki, and R. Shindou, Effect of Disorder in a Three-Dimensional Layered Chern Insulator, Phys. Rev. Lett. 116, 066401 (2016).
- [19] S. Bera, J. D. Sau, and B. Roy, Dirty Weyl semimetals: Stability, phase transition, and quantum criticality, Phys. Rev. B **93**, 201302(R) (2016).
- [20] H. Shapourian and T. L. Hughes, Phase diagrams of disordered Weyl semimetals, Phys. Rev. B 93, 075108 (2016).
- [21] A. Altland and D. Bagrets, Theory of the strongly disordered Weyl semimetal, Phys. Rev. B **93**, 075113 (2016).
- [22] S. V. Syzranov, P. M. Ostrovsky, V. Gurarie, and L. Radzihovsky, Critical exponents at the unconventional disorderdriven transition in a Weyl semimetal, Phys. Rev. B 93, 155113 (2016).
- [23] T. Louvet, D. Carpentier, and A. A. Fedorenko, On the disorder-driven quantum transition in three-dimensional relativistic metals, Phys. Rev. B 94, 220201(R) (2016).
- [24] J. H. Pixley, D. A. Huse, and S. Das Sarma, Rare-Region-Induced Avoided Quantum Criticality in Disordered Three-Dimensional Dirac and Weyl Semimetals, Phys. Rev. X 6, 021042 (2016).
- [25] J. H. Pixley, D. A. Huse, and S. Das Sarma, Uncovering the hidden quantum critical point in disordered massless Dirac and Weyl semimetals, Phys. Rev. B 94, 121107(R) (2016).
- [26] B. Sbierski, K. A. Madsen, P. W. Brouwer, and C. Karrasch, Quantitative analytical theory for disordered nodal points, Phys. Rev. B 96, 064203 (2017).
- [27] J. H. Pixley, Y.-Z. Chou, P. Goswami, D. A. Huse, R. Nandkishore, L. Radzihovsky, and S. Das Sarma, Single-particle excitations in disordered Weyl fluids, Phys. Rev. B 95, 235101 (2017).
- [28] V. Gurarie, Theory of avoided criticality in quantum motion in a random potential in high dimensions, Phys. Rev. B **96**, 014205 (2017).
- [29] T. Holder, C.-W. Huang, and P. M. Ostrovsky, Electronic properties of disordered Weyl semimetals at charge neutrality, Phys. Rev. B **96**, 174205 (2017).

- [30] J. H. Wilson, J. H. Pixley, P. Goswami, and S. Das Sarma, Quantum phases of disordered three-dimensional Majorana-Weyl fermions, Phys. Rev. B 95, 155122 (2017).
- [31] J. H. Wilson, J. H. Pixley, D. A. Huse, G. Refael, and S. Das Sarma, Do the surface Fermi arcs in Weyl semimetals survive disorder? Phys. Rev. B **97**, 235108 (2018).
- [32] K. Ziegler and A. Sinner, Short Note on the Density of States in 3D Weyl Semimetals, Phys. Rev. Lett. **121**, 166401 (2018).
- [33] M. Buchhold, S. Diehl, and A. Altland, Vanishing Density of States in Weakly Disordered Weyl Semimetals, Phys. Rev. Lett. 121, 215301 (2018); Nodal points of Weyl semimetals survive the presence of moderate disorder, Phys. Rev. B 98, 205134 (2018).
- [34] I. Balog, D. Carpentier, and A. A. Fedorenko, Disorder-Driven Quantum Transition in Relativistic Semimetals: Functional Renormalization via the Porous Medium Equation, Phys. Rev. Lett. 121, 166402 (2018).
- [35] J. Klier, I. V. Gornyi, and A. D. Mirlin, From weak to strong disorder in Weyl semimetals: Self-consistent Born approximation, Phys. Rev. B **100**, 125160 (2019).
- [36] J. H. Pixley, J. H. Wilson, D. A. Huse, and S. Gopalakrishnan, Weyl Semimetal to Metal Phase Transitions Driven by

- Quasiperiodic Potentials, Phys. Rev. Lett. **120**, 207604 (2018).
- [37] H. Nielsen and M. Ninomiya, A no-go theorem for regularizing chiral fermions, Phys. Lett. B 105, 219 (1981); Absence of neutrinos on a lattice: (I). Proof by homotopy theory, Nucl. Phys. B 185, 20 (1981); Absence of neutrinos on a lattice: (II). Intuitive topological proof, 193, 173 (1981).
- [38] B. Sbierski and C. Fräßdorf, Strong disorder in nodal semimetals: Schwinger-Dyson-Ward approach, Phys. Rev. B 99, 020201(R) (2019).
- [39] See Supplemental Material at http://link.aps.org/supplemental/ 10.1103/PhysRevB.102.100201 for further finite size data on both the cubic and fcc lattices, extra analysis on the observed rare state, and self-consistent Born approximation calculations.
- [40] Y.-Z. Chou and M. S. Foster, Chalker scaling, level repulsion, and conformal invariance in critically delocalized quantum matter: Disordered topological superconductors and artificial graphene, Phys. Rev. B **89**, 165136 (2014).
- [41] A. Weiße, G. Wellein, A. Alvermann, and H. Fehske, The kernel polynomial method, Rev. Mod. Phys. **78**, 275 (2006).
- [42] http://hpcc.umd.edu.
- [43] http://oarc.rutgers.edu.